ACS APPLIED MATERIALS & INTERFACES

Research Article

www.acsami.org

Controlled Drug Release and Hydrolysis Mechanism of Polymer–Magnetic Nanoparticle Composite

Fang Yang,[†,§] Xiaoxian Zhang,*[,‡,§] Lina Song,[†] Huating Cui,[†] John N. Myers,[‡] Tingting Bai,[†] Ying Zhou,[†] Zhan Chen,*[,‡] and Ning Gu*[,†]

[†]State Key Laboratory of Bioelectronics, Jiangsu Key Laboratory for Biomaterials and Devices, School of Biological Science & Medical Engineering, Southeast University, Nanjing, 210096, P. R. China

[‡]Department of Chemistry, University of Michigan, 930 North University Avenue, Ann Arbor, Michigan 48109, United States

Supporting Information

ABSTRACT: Uniform and multifunctional poly(lactic acid) (PLA)–nanoparticle composite has enormous potential for applications in biomedical and materials science. A detailed understanding of the surface and interface chemistry of these composites is essential to design such materials with optimized function. Herein, we designed and investigated a simple PLA–magnetic nanoparticle composite system to elucidate the impact of nanoparticles on the degradation of polymer–nanoparticle composites. In order to have an in-depth understanding of the mechanisms of hydrolysis in PLA–nanoparticle composites, degradation processes were monitored by several surface sensitive techniques, including scanning electron microscopy, contact angle goniometry, atomic force microscopy, and sum frequency generation spectroscopy. As a second-order nonlinear optical technique, SFG spectroscopy was introduced to directly probe in situ chemical nature at the PLA–magnetic nanoparticle composite/aqueous interface, which allowed for the delineation of molecular mechanisms of various hydrolysis processes for degradation at the molecular level. The best PLA–NP material, with a concentration of 20% MNP in the composite, was found to enhance the drug release rate greater than 200 times while maintaining excellent controlled drug release characteristics. It was also found that during hydrolysis, various crystalline-like PLA domains on the surfaces of PLA–nanoparticle composites influenced various hydrolysis behaviors of PLA. Results from this study provide new insight into the design of nanomaterials with controlled degradation and drug release properties, and the underlined molecular mechanisms. The methodology developed in this study to characterize the polymer–nanoparticle composites is general and widely applicable.

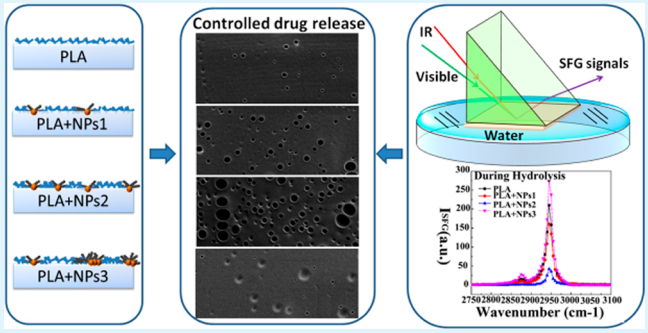

KEYWORDS: *poly(lactic acid), nanoparticles, composite, sum frequency generation, interface hydrolysis, controlled drug release*

1. INTRODUCTION

Poly(lactic acid) (PLA), a well-known biodegradable polymer, has been extensively studied in the past few decades because it is hydrolytically degradable and its byproducts are nontoxic.[1−3] For biomedical and pharmaceutical applications, PLA, prepared as films, microparticles, microrods, and other forms, has been commercialized as pharmaceutical adjuvants for drug delivery, tissue engineering, and surgical implants.[4−6] Since PLA has been proven to be useful in a wide range of controlled drug delivery applications, utilizing biodegradable PLA in composite or hybrid systems with other biodegradable or nondegradable materials is more promising as multifunctional biomedical delivery carriers. Nowadays, many therapeutic agents, various NPs, and different proteins have been encapsulated within PLA as drug delivery vehicles to achieve multifunction.[7,8] In particular, a variety of biomedical nanoparticles (NPs) have been embedded in PLA polymers to form polymer–NP composites to pursue new biomedical applications.[9] For instance, superparamagnetic iron oxide Fe_3O_4 NPs (SPIO), CdTe quantum dots (QDs), and gold NPs have been surface-modified and combined with PLA polymers for biomedical imaging, cell labeling, and therapy.[10−13] In our previous work, the PLA encapsulated microbubbles embedded with SPIO NPs were found to be effective as ultrasound and magnetic resonance dual contrast agents.[14,15] Additionally, the SPIOs with PLA coating were reported to be both magnetic field responsive and useful as drug delivery systems.[16] Therefore, the PLA–NP composite may provide possibilities for combining the desirable characteristics of PLA with that of NPs, leading to controlled drug delivery formulations for an even wider range of biomedical applications.

Biodegradable PLA polymers have been of interest in controlled release technology for a long time because they can be absorbed by the body. Especially, the release rate and

Received: October 7, 2014
Accepted: April 16, 2015
Published: April 16, 2015

DOI: 10.1021/acsami.5b02210
ACS Appl. Mater. Interfaces 2015, 7, 9410−9419

profile of a PLA−NP hybrid system is of great importance for biomedical applications.[17−19] That is, degradation, i.e., hydrolysis of PLA, which is directly related to the release property of a PLA−NP composite, is vital for a controlled PLA drug delivery system. Many factors, e.g., the molecular weight,[20] chemical modification,[21] and the introduction of other agents into the polymer network,[22] could influence the release behavior. Although the degradability of PLA itself has been extensively characterized,[23−26] most of the investigations were primarily focused on the bulk studies. Molecular mechanisms of hydrolysis of PLA materials, especially PLA−NP composites, remain poorly understood. The chemical mechanisms of PLA−NP hybrid degradation at the molecular level are not well understood, which may hinder the rational design of PLA materials in applications that require careful control over the degradation rate. Moreover, we also believe that understanding the degradability of PLA near the interface can be equally (or even more) important for applications of PLA materials in real biological systems because the PLA molecules first contact and interact with the surrounding liquid environment at the PLA/surrounding interface.

In this study, a simple polymer−NP composite system was designed and investigated to elucidate the impact of NPs on the surface degradation of polymer−NP composite and to correlate the surface and bulk degradation mechanism to the corresponding drug release rate. Specifically, PLA and Fe_3O_4 magnetic NPs (MNPs) were chosen in this research to form PLA−MNP composites with various MNP concentrations, which permit the investigation of the influence of MNPs on PLA degradation at the molecular level. The degradation process was examined by multiple techniques including scanning electron microscopy (SEM), atomic force microscopy (AFM), and contact angle goniometry (CA). Especially, a nonlinear optical technique, sum frequency generation vibrational spectroscopy (SFG), was introduced to directly probe the molecular structure changes at the PLA−MNP composite/liquid interface in situ, which has been developed into a powerful tool to study the interfacial molecular structures of polymers and biomolecules.[27−31] Molecular level information detected by SFG together with SEM, AFM, and CA measurements allowed us to explore the molecular mechanisms to interpret the various hydrolysis behaviors of PLA−MNP composites. Concomitantly, we loaded a hydrophobic drug, paclitaxel (PTX), into the PLA−MNP composites to correlate the drug release rate to the polymer composite hydrolysis behavior. The in-depth understanding of the degradation process of the PLA−MNP composite will aid in the design of future drug delivery systems with improved properties and make full use of the properties of PLA and MNPs to achieve multifunction in biomedical applications eventually. Also, the methodology developed here to investigate the hydrolysis process of the PLA−MNP composite system at the molecular level is general and can be extended to study other polymer-NP systems.

2. MATERIALS AND METHODS

2.1. Materials. PLA ($M_w \approx 42$ kDa) was supplied by Phusis (U.S.A.). Paclitaxel (PTX, analytical standard) was purchased from Aladdin Industrial Corporation (Shanghai, China). The Fe_3O_4−MNPs (mean diameter of ∼12 nm) with oleic acid on the surfaces were provided by Jiangsu Laboratory for Biomaterials and Devices (Jiangsu, China). Chloroform ($CHCl_3$, ≥ 99.9% purity) and deuterium oxide (D_2O, 99.9 atom % D) were obtained from Sigma-Aldrich (St. Louis, Mo, U.S.A.). All chemicals were used as received. The molecular structures of PLA and oleic acid coated on MNPs surfaces are shown in Figure 1.

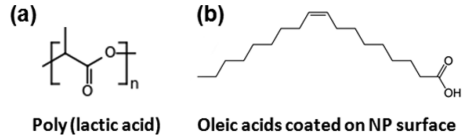

Figure 1. Molecular structures of PLA (a) and oleic acid (b) coated on MNP surfaces are shown.

2.2. Preparation of PLA−MNPs Composites. First, PLA (0.50 g) was mixed with hydrophobic MNPs of different weights in $CHCl_3$ at room temperature (∼25 °C). Three MNP concentrations were selected with the PLA/MNPs mole ratios of 50:1 (∼2% MNPs), 5:1 (∼20% MNPs), and 1:1 (50% MNPs), and the corresponding samples were referred to PLA−NPs1, PLA−NPs2, and PLA−NPs3, respectively, in the article. Pure PLA was also studied as a control. PLA and MNPs were thoroughly mixed in solution using a vortex mixer (Vortex-Genie 2T, Scientific Industries Inc.) until the solutions appeared clear. For PTX loading in the four kinds of samples (pure PLA plus three PLA−MNPs mixtures), the PTX solution was evenly dispersed in the above-mentioned pure PLA solution and various PLA−MNP mixture solutions.

Second, films of pure PLA and three PLA−MNP mixtures with different MNP concentrations, as well as the mixtures loaded with PTX were prepared by spin-coating (3000 rpm, 30 s) using a P-6000 spin-coater (Speedline Technologies). The concentration of MNPs embedded in the film before and after the spin coating process was determined by an Atomic Absorption Spectrometer (180−80 Hitachi, Japan) to confirm MNP concentration. The results show that the MNP concentration does not change after spin coating. And the high-performance liquid chromatography (HPLC) was also used to determine the amounts of PTX in the film before and after the spin coating process, which indicated the same PTX concentration after spin coating. Except for the SEM study, fused silica windows (ESCO Products, Inc., U.S.A.) were utilized as substrates to prepare sample films for all of the following measurements. For the SEM study, sample films were deposited on the Si wafer surfaces using the above method. Since Si wafer surfaces are actually silica, we believe that the silica wafer and fused silica surfaces are similar and therefore the deposited films are the same. In addition, to enhance the SFG signal detected from the polymer/water interface, fused silica prisms were also utilized as substrates for film deposition.[28,32] Both SFG sample geometries used in this study with fused silica window (referred to as window geometry) and fused silica prism (referred to as prism geometry) are displayed in Figure 2.

The spin-coated films were then placed in a vacuum chamber overnight to remove the residual solvent. The thicknesses of all the films were measured by a depth profilometer (Dektak6M Stylus Surface Profilometer, Veeco) to be around 200 nm. The film thicknesses were almost unchanged after hydrolysis for 1 h.

Next, for SEM, AFM, and CA measurements, the PLA and PLA−MNPs hybrid films were dipped into milli-Q water (18.2 MΩ, Millipore) and the measurements were taken before and after different hydrolysis times, including 1, 39, and 60 h. For SFG experiments, the in situ SFG spectra from the film/water interface as well as those from film surfaces in air before and after water exposure were collected. D_2O was used for SFG experiments on film/water interfaces to avoid spectral confusion.

2.3. Scanning Electron Microscopy. The surface morphologies of the PLA and PLA−MNP hybrid films were studied by scanning electron microscopy (SEM, JEOL JSM-840A, Japan) before and after short-term (1 h) and long-term (39 and 60 h) hydrolysis. An accelerating voltage of 1 kV was used at a working distance of 2.5 mm.

2.4. Atomic Force Microscopy. The phase image of tapping mode atomic force microscopy (AFM, Agilent, PicoPlus, Japan) could be a useful tool to reveal the MNP distribution and/or clusters

DOI: 10.1021/acsami.5b02210
ACS Appl. Mater. Interfaces 2015, 7, 9410−9419

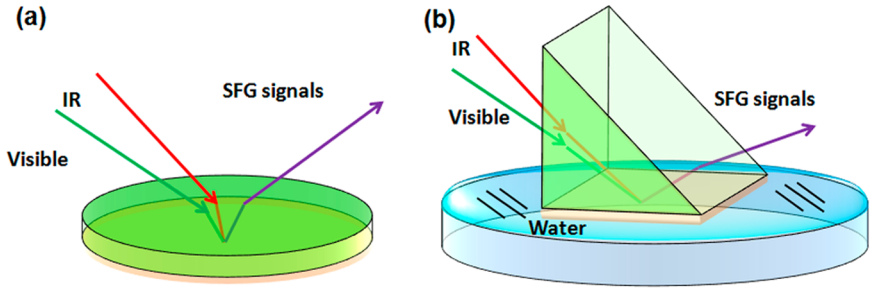

Figure 2. Two SFG geometries, window face-down geometry (a) and prism near total internal reflection geometry (b) were utilized in this study.

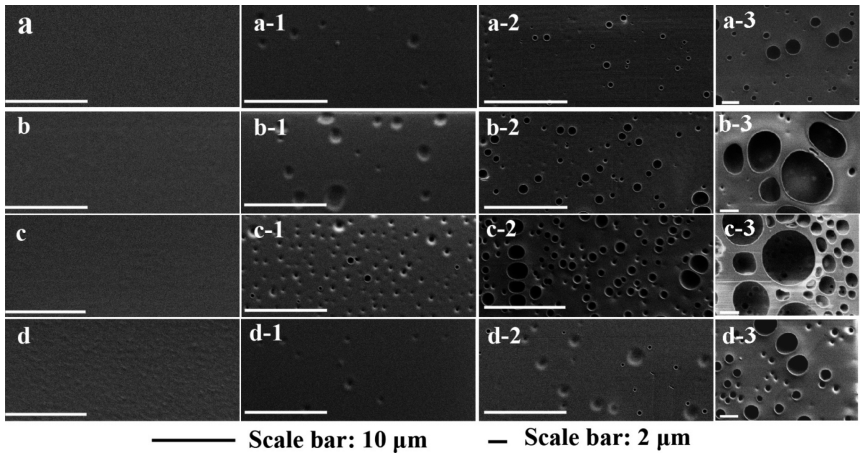

Figure 3. SEM images of pure PLA (a) and PLA−MNP hybrid films with various MNP bulk concentrations ((b) ∼2%, (c) ∼20% and (d) ∼50%) before contact with water. Images labeled as a-1, b-1, c-1, and d-1 and those labeled as a-2, a-3, b-2, b-3, c-2, c-3, d-2, and d-3 are SEM images of various films of a, b, c, and d after immersion in water for 1, 39, and 60 h, respectively, for hydrolysis.

embedded in the polymer film. The surface change images were realized with AFM. A silicon cantilever was used for all measurements. The spring constant of the cantilever of taping probe (NSC 14/AIBS, Ultrashape, Estonia) was 1.8−12.5 N/m. Typically, the surface morphology of 20 × 20 μm^2 area near the center of each sample was observed by using the tapping mode of the scanning probe.

2.5. Contact Angle. Static water contact angle (CA) measurements were performed using a CAM 100 Optical Contact Meter (KSV Instruments, Finland). Each water contact angle reported was determined by averaging the measured angles on at least three samples, each sample with five measurements on five different spots, while the measured contact angle on each spot is calculated by averaging the angles deduced from ten pictures taken from the water drop on that spot. The mean value with the standard deviation of the contact angle was reported.

2.6. SFG Experiment. The SFG setup used in this research is a commercially available system from EKSPLA. The optical setup has been reported in detail previously.[27−29,33] The ssp (s-polarized signal output, s-polarized visible input, and p-polarized IR input) polarization combination was utilized for all SFG spectra. SFG spectra were measured by using both window geometry and prism geometry (Figure 2). Notice that for all the SFG spectra labeled as "before and after hydrolysis", all the spectra were collected from air/film interfaces, while for all the spectra labeled as "during hydrolysis", all the spectra were collected from water/film interfaces.

2.7. In Vitro Drug Release Studies. The in vitro release of PTX from the PTX loaded PLA−MNP hybrid films to the surrounding media was evaluated to better understand the effect of the changes/hydrolysis of the films on drug-release. Tween-20 (0.05%) in phosphate buffered saline (PBS, pH = 7.4) was utilized as the release media. The PTX loaded hybrid films were immersed in 2 mL of PBS/Tween-20 and incubated in a circulating water bath (Thermo Scientific, U.S.A.) at 37 °C. Tween-20 is a nonionic surfactant that is commonly added to PBS to increase the solubility of PTX and maintain sink conditions. After immersion for different times (0.5, 1, 1.5, 6, 39, and 60 h), the film samples were removed from the solution. Then the PBS/Tween-20 solutions were analyzed quantitatively using high-performance liquid chromatography (HPLC) to determine the amounts of PTX released to the solutions. The cumulative release rate of PTX from the film then was calculated based on the total loading PTX concentration.

The HPLC (Waters e2695 system, U.S.A.) used in this study is equipped with a Waters 2489 UV—vis detector and a Nova-Pak C18 column (3.9 × 150 mm^2; 4 μm particle size). Briefly, a mobile phase of water and acetonitrile mixture (45:55, Volume/Volume) was used at a flow rate of 1 mL/min. An injection volume of 10 μL was used for the analysis. The column temperature was maintained at 25 °C. The UV detector wavelength was set at 227 nm. Waters Millennium32 software was used to analyze the collected HPLC data.

3. RESULTS AND DISCUSSION

3.1. SEM and AFM Results. SEM was performed to monitor the surface morphology of PLA−MNP hybrid films with various bulk MNP concentrations after immersion in water for different times to understand the surface appearance changes. Figure 3 shows SEM images exhibiting surface morphology of PLA and PLA−MNP hybrid films before and after short-term (1 h) and long-term (39 h, 60 h) immersion in water for hydrolysis. Before water immersion, the surfaces of all the spin-coated films were more or less smooth (Figure 3a−d), indicating that the surfaces were morphologically homogeneous. However, after immersing the samples into water for 1 h, pores with various sizes and densities appeared on all the surfaces (Figure 3a-1−d-1), suggesting that hydrolysis occurred on all the film surfaces. The quantitative information on the pore size and density on the surfaces of the four samples (PLA,

DOI: 10.1021/acsami.5b02210
ACS Appl. Mater. Interfaces 2015, 7, 9410−9419

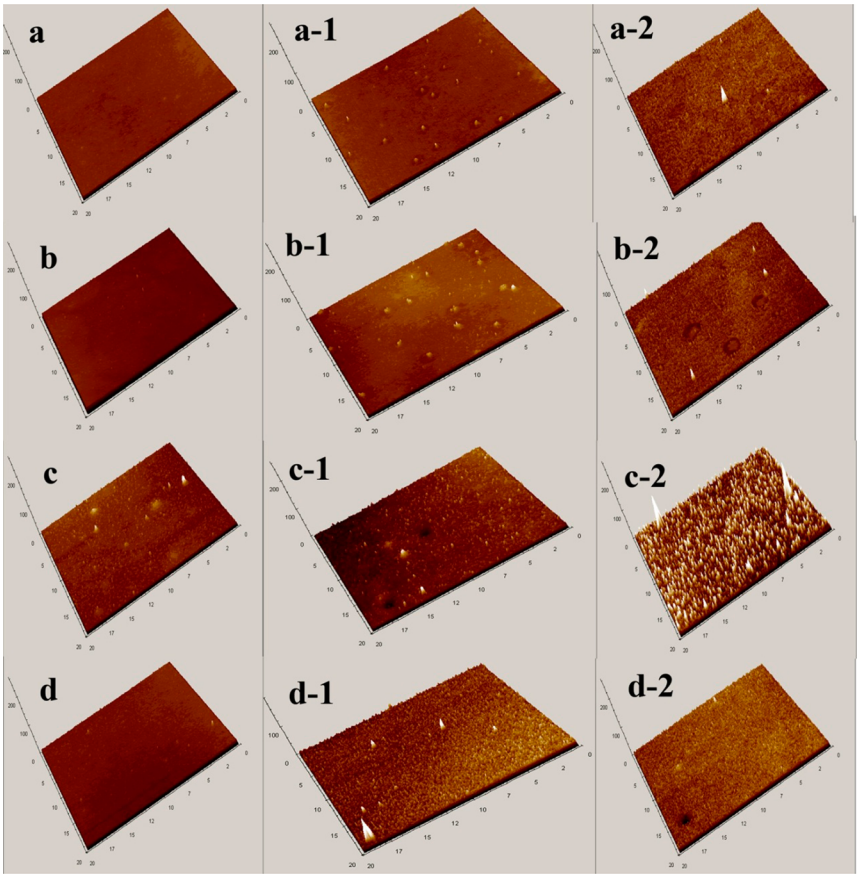

Figure 4. AFM 3D representative images of pure PLA (a) and PLA−MNP hybrid films with various MNP bulk concentrations ((b) ∼2%, (c) ∼20%, and (d) ∼50%) before contact with water. Images labeled as a-1, b-1, c-1, and d-1 and those labeled as a-2, b-2, c-2, and d-2, are AFM images of various films of a, b, c, and d after immersion in water for 39 and 60 h, respectively, for hydrolysis.

composite with 2% MNP or PLA−NPs1, composite with 20% MNP or PLA−NPs2, composite with 50% MNP or PLA−NPs3) after immersion in water for 1, 39, and 60 h for hydrolysis is shown in SI Table S1.

The images detected after 1 h hydrolysis clearly show that the PLA hydrolysis more likely occurred by forming pores on the surface rather than layer-by-layer etching. With the increase of the MNP concentration in the PLA films from zero (pure PLA) to ∼2% to ∼20%, pores with bigger sizes (from 1.65 to 2.44 μm) and higher densities (from 0.12 to 0.39 pores per μm^2) were observed on the surfaces, indicating that the PLA surface hydrolysis rate increased by increasing the MNP concentrations in the PLA films (Figures 3b-1, 1c-1). However, as the concentration of MNPs further increased to 50%, less pores with relatively smaller sizes were observed on the surface of PLA−NPs3 (Figure 3d-1), showing that the hydrolysis rate decreased under the same condition. These results suggest that the hydrolysis on the PLA surfaces can be significantly influenced by the bulk concentration of MNPs. Similar trends were observed in all of the films after hydrolysis for 39 h (Figures 3a-2−d-2), but with higher pore densities on each surface. After hydrolysis for 60 h (Figures 3a-3−d-3), although the pore densities did not significantly increase, the pore size indeed became larger (SI Table S1). Besides, when MNP concentration reached 20% in the PLA film, some smaller pores can be found in the big pores.

AFM is a common microscopic method to investigate the surface morphology of polymers and polymer composites. 3D representative images shown in Figure 4 have been created from the topography images. The addition of MNPs in the film increases the surface roughness. More MNPs in the film made the surface rougher (Figure 4a−d). After 1 h hydrolysis, surface morphologies are similar to those before hydrolysis samples just the roughness increased, which is shown in SI Figure S1 of AFM phase images of these four samples. After hydrolysis 60 h, the pores were found and the trend is similar to the SEM results in Figure 3. Even at the concentration of 20%, except pore formation, the surface wettability also significantly increased shown in Figure 4(c-2).

From both SEM and AFM results, we can see that the PLA hydrolysis can occur on the film surfaces by forming pores and MNPs embedded in the PLA network can strongly affect the hydrolysis rate. In addition, the concentration of MNPs in bulk was found to play an important role in hydrolysis. MNPs with lower concentrations (2%- 20%) in PLA appear to act as catalysts and are capable of accelerating the hydrolysis. As the concentration of MNPs went up to 50%, the hydrolysis rate of PLA could be increased, but not as much as that of the low concentration MNP case early in the process. The hydrolysis rate increased more later, as demonstrated by the results from the sample after water immersion for 39 and 60 h.

3.2. Contact Angle Measurement Results. In order to further elucidate the effects of MNPs on PLA hydrolysis and clarify the molecular mechanisms, static CA tests were conducted on the PLA and PLA−MNPs hybrid films before, during, and after immersion in water for hydrolysis. CA measurements, reporting the surface hydrophilicity and wettability, were carried out on the PLA films to address the

DOI: 10.1021/acsami.5b02210
ACS Appl. Mater. Interfaces 2015, 7, 9410−9419

Table 1. CA Results of PLA and PLA−MNPs Hybrid Films before and after Hydrolysis for 39 and 60 h

samples	before hydrolysis (deg.)	after hydrolysis 39 h (deg.)	after hydrolysis 60 h (deg.)
PLA	78.3 ± 2.4	76.8 ± 1.2	72.1 ± 1.4
PLA−NPs1	77.3 ± 2.5	75.4 ± 2.1	71.1 ± 2.1
PLA−NPs2	70.8 ± 1.7	68.5 ± 2.5	67.3 ± 2.3
PLA−NPs3	73.4 ± 1.6	72.5 ± 1.5	71.4 ± 2.4

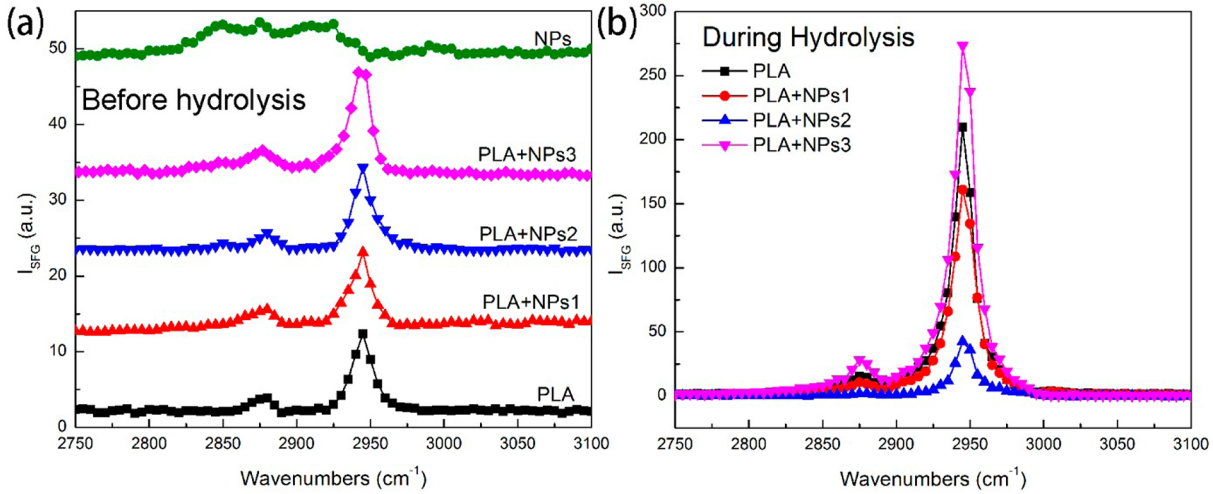

Figure 5. SFG ssp spectra collected from the surfaces of pure PLA and PLA−MNP hybrid films before (a) and during the water immersion (b). Prism geometry was used here. In (a), the spectra are offset for clarity.

possible hydrolysis mechanisms of PLA−MNP hybrid systems. The CAs of the original films before hydrolysis (Table 1) were different for different MNP bulk concentrations, indicating that the sample surface hydrophilicity is dependent on the concentration of MNPs in the PLA bulk. In addition, the surface CA changes are not monotonic, well correlated to the hydrolysis behavior observed with SEM and AFM above. That is, as the bulk MNP concentration increased from zero to ∼2%, the measured CA reduced from ∼78.3 ° to ∼77.3°. Then, as the bulk MNP concentration continued to increase to ∼20%, the CA further decreased to ∼70.8°. As the bulk NP concentration increased further to 50%, the CA increased (instead of decreasing) to ∼73.4°. The reason may be that when hydrophobic MNPs were introduced into the film, because of the hydropobic−hydrophobic interaction between PLA and MNPs, the macro-structured surface had better wettability. More detailed discussion will be done later by combining SFG results. Here, with the time increase of hydrolysis, the CA decreased gradually for each sample. Especially after hydrolysis 39 and 60 h, both SEM and AFM results indicated pyramids and pores emerged on the film surface, which is beneficial for creating hierarchically micro/nano-roughened surfaces. Such hierarchically micro/nano-roughened surfaces have been reported to lead to hydrophobicity.[34] Therefore, the surface wettability changes characterized by measured CA changes for PLA−MNP composite films are likely related to their various initial hydrolysis behaviors. Better surface wettability (with lower water CAs) may induce better water contact/interaction thus result in easier or faster hydrolysis reactions on the film surface. This can explain the observed SEM and AFM results: the hydrolysis increased from PLA to PLA−NPs1 to PLA−NPs2, and then deceased from PLA−NPs2 to PLA−NPs3. However, the comparison between PLA and PLA−NPs3 (the 50% MNP in PLA sample) shows an exception. As the bulk MNP concentration increased from 0 to 50%, the measured CA decreased from ∼78.3° to ∼73.4°.

The time-dependent CA data indicated that as the water immersion time increased from zero to 39 to 60 h, the CA reduced for all films except for the PLA−NPs3 film (with 50% MNP, which CAs were almost not changed). These trends can be seen more clearly in SI Figure S2.

3.3. SFG Results. In order to further elucidate the hydrolysis mechanisms of PLA−MNP composites at the molecular level, a surface-sensitive technique, SFG, was utilized to investigate the molecular structural changes on the PLA and PLA−MNP hybrid film surfaces. First, surface molecular structures were probed by SFG to study the surface variations of PLA and various PLA−MNPs hybrid films before water immersion. We can see from Figure 5a that before water immersion for hydrolysis, the SFG spectral features from different sample surfaces are similar, only with slightly different peak intensities. Two main peaks (near 2880 and 2945 cm^{-1}) in the spectra can be assigned to methyl symmetric stretching and methyl Fermi resonance, respectively.[27−29,33,35] In the case of PLA−NPs2 and PLA−NPs3 films, additionally, a small peak around 2850 cm^{-1}, which could be generated from the symmetric CH_2 stretch, was detected by SFG as well. Because PLA has no methylene group, this methylene signal can be assigned to the CH_2 chains in oleic acids coated on MNP surfaces (Figure 1a,b). This was confirmed by a similar peak observed in the SFG spectrum detected from the pure MNPs coated on a SiO_2 prism (Figure 5a). For MNPs, if MNPs have a perfect centro-symmetric structure and oleic acid molecules were coated homogeneously on MNP surfaces, then no SFG signals should be observed (according to the SFG selection rule that only a medium with no inversion symmetry can generate SFG signal under the electric dipole approximation). However, some SFG signals with broad features (completely different from those detected from PLA−MNP composites) were

DOI: 10.1021/acsami.5b02210
ACS Appl. Mater. Interfaces 2015, 7, 9410−9419

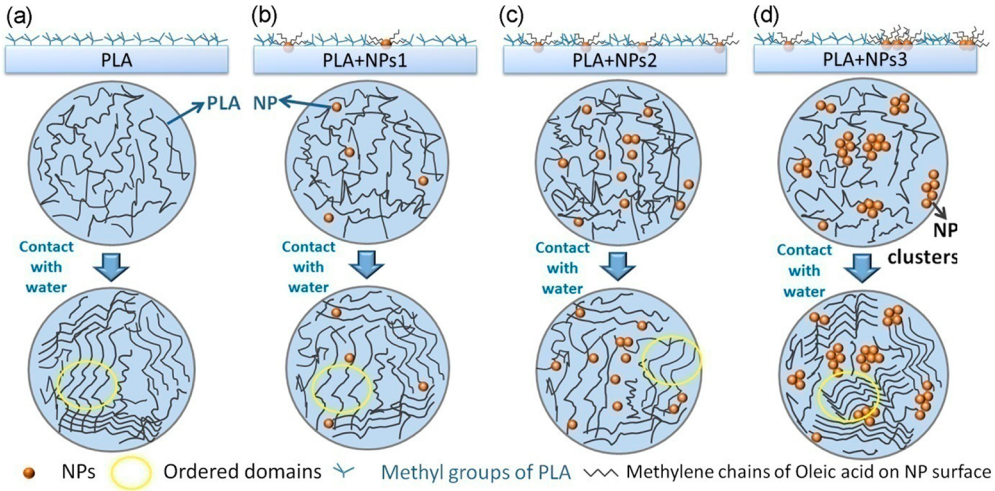

Figure 6. Schematics showing PLA surface structural changes while contacting water for pure PLA (a), and PLA−MNP composites with ∼2% (b), ∼20% (c) to 50% (d) MNPs in the film bulk. The sizes of PLA and NPs were not drawn to scale.

detected. Such SFG signals should be generated from vibrational modes of CH_2/CH_3 groups due to inhomogeneous coatings or noncentrosymmetric MNP shapes, as well as nonresonant background induced by Fe_3O_4 MNPs (Figure 5a).[36] These results demonstrate that even when the MNP bulk ratio reached 50%, no obvious MNP SFG signals could be observed (while only a minimal CH_2 peak detected from the composite samples containing 20% and 50% MNPs), indicating that the surfaces of PLA hybrid films were mostly covered by PLA molecules but not MNPs coated with oleic acids.

In the SFG spectra, despite of the similar peak intensity ratios, as the MNP concentration increased from zero to ∼2%, the peak intensities reduced. Similar lower peak intensities could also be observed from the PLA−NPs2 spectra (∼20% MNPs in Figure 5a). However, as the MNP concentration increased further to 50%, the peak intensities became higher again, similar to those of the pure PLA film (Figure 5a). Similar SFG results were observed from the samples deposited on SiO_2 windows, showing that the SFG data collected from both the window and prism geometries are comparable and dominated by contributions from sample surfaces instead of buried film/substrate interfaces (Figure 5a and SI Figures S3a−d).[37] This observed nonmonotonic SFG signal intensity variation trend for different samples (with different MNP concentrations) is consistent with the SEM (variation trend for surface pore size and density) and CA (variation trend for surface wettability) results. The SFG peak intensity decrease as a function of MNP concentration (increased from 0 to 20%) can be interpreted by the fact that the surface can be more disordered and/or with less CH_3 groups. As the MNP concentration further increased to 50%, a more ordered surface and/or the presence of more CH_3 groups on the surface was induced by larger amounts of MNPs in the sample.

Subsequently, SFG measurements were also performed on PLA and PLA−MNP hybrid films after water immersion for hydrolysis for 1 and 39 h. Since similar SFG results were obtained after water immersion for 60 h, only SFG results of 1 and 39 h water immersion were shown. Compared to the SFG spectra before water immersion, no substantial surface structure changes were detected by SFG after water immersion (SI Figures S3a−d).

To further investigate the details about various hydrolysis processes of PLA−MNP hybrid films and the effects of the bulk MNP concentration on the hydrolysis, in situ SFG measurements were carried out on the surfaces of pure and hybrid PLA films in contact with water (Figure 5b). Surprisingly, for all samples, the SFG intensities increased dramatically despite the similar spectral features as the surfaces contacted D_2O. Figure 5b also shows that the intensities of SFG spectra varied significantly although they all dramatically increased during the water contact. For pure PLA, the SFG intensity from the surface in water was 22 times higher than that detected in air. For the PLA film with ∼2% MNPs, the SFG intensity from the surface in water was 15 times larger than that detected in air. Interestingly, as the MNP ratio in the PLA film bulk increased to ∼20%, the SFG intensity from the surface in water was only three times higher compared to that detected in air. As the NP concentration increased to 50%, SFG intensity detected from the surface in water increased dramatically again and was 27 times larger than that in air. The above observed SFG signal changes can be explained by the following possible reasons: (1) more ordered PLA and PLA−MNP composite surfaces (or bulk if the signal contains bulk contribution), (2) an increase in number of molecules detected, and/or (3) a change in the Fresnel coefficients due to a change in index of refraction from air to water. If the Fresnel coefficient is the only reason, then the signal intensity should only increase several times, not more than 20 times as observed. Besides, it is unlikely that the molecular amounts of PLA−MNPs would increase that much after in contact with water. Therefore, the observed signal increase seen in Figure 4b must mainly be due to the first factor outlined above, that is, the formation of highly order structures on the surface.

Therefore, we believe that the SFG results shown in Figure 5b suggest that PLA molecules still covered the film surfaces during the hydrolysis process and highly ordered structures of PLA were formed on the film surfaces while in contact with water. Since PLA can form crystalline structures easily, the SFG signal increase can be explained by the formation of PLA crystalline-like structures on the surfaces in the presence of water molecules. Although relatively high temperatures, such as 80 °C,[9,38] are normally required to generate crystalline PLA films, the existence of water molecules in the systems may

DOI: 10.1021/acsami.5b02210
ACS Appl. Mater. Interfaces 2015, 7, 9410−9419

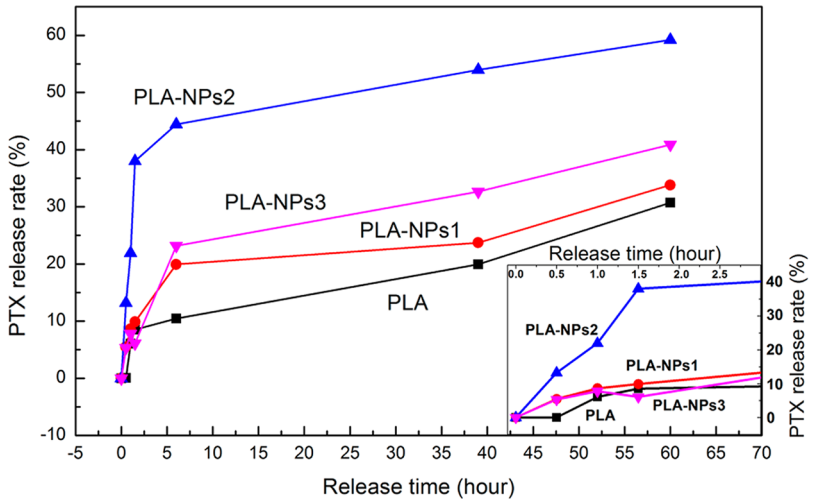

Figure 7. PTX release rate as a function of release time for PLA and PLA−MNP hybrid films.

lower the crystallization activation energy and thus cause the formation of crystalline-like structures on the film surfaces.

However, after removing the samples from water, the SFG intensities detected from various sample surfaces in air recovered (SI Figure S3). This suggests that pure and composite PLA films are not "fully" crystallized in water, otherwise the crystallized systems would be very stable and would not be able to return to the original amorphous states so quickly. Therefore, we believe that the highly ordered structures or crystalline-like structures in PLA and PLA−MNP hybrid films should only occur on or near the surface but not throughout the entire film.

According to the previous study,[39] SFG signals contributed by the crystalline domains could be much stronger than that by the amorphous portion of the films. Therefore, the SFG intensities observed could be correlated to the surface crystallinity of PLA films. The stronger the SFG intensities were, the higher surface crystallinity of PLA films could be. It is interesting to see that the trend of SFG signal intensity variation for different samples with different MNP bulk concentrations is quite consistent with the SEM and CA results, which can be explained by the surface crystallization hypothesis we proposed above. Previous studies demonstrated that PLA crystalline structures were more resistant against water hydrolysis compared to amorphous structures.[40,41] Therefore, the molecular mechanisms of various hydrolysis behaviors on pure and hybrid PLA films can be illustrated schematically in Figure 6. For pure PLA, the film surface is dominated by CH_3 groups and the surface CA is ∼78.3°, thus the surface is fairly hydrophobic and has relatively poor water wettibility. When in contact with water, the surface water interactions might lower the local crystallization energy barrier of PLA and thus facilitate the formation of crystalline-like highly ordered structures on the film surface (Figure 6a), which would further decrease the hydrolysis rate of PLA. Therefore, due to the surface hydrophobicity and crystallinity, the intrinsic hydrolysis rate of pure PLA film should be quite slow. As the MNP ratio in bulk increased to ∼2% (Figure 6b), the hydrophobic−hydrophobic interaction between PLA and oleic acids (on MNP surfaces) might induce a small part of methyl groups from PLA to change surface orientation to lie down parallel to the film surface. That is, less methyl groups would be ordered vertically on the film surface compared to pure PLA, which decreased the surface CA from ∼78.3° to ∼77.3° and thus slightly increased the water wettibility on the film surface. This can be confirmed by the lower peak intensities in SFG spectra compared to pure PLA (SI Figure S3a,b). Besides, the dispersion of more MNPs in PLA network may disturb the PLA chain ordering, thus reduce the crystallinity of PLA on the surface, leading to relatively weaker peaks in the PLA−NPs1 SFG spectrum observed in water (Figure 5b). Although the formation of crystalline-like structures inhibited the hydrolysis of PLA to some degree, compared to pure PLA, the increased surface wettibility and lower crystallinity level of PLA on the surface of PLA−NPs1 film worked together to make the PLA hydrolysis faster than that of pure PLA.

Similar explanations could be used to elucidate the observed hydrolysis of PLA−NPs2 film. Adding ∼20% MNPs to the PLA film bulk leads to more MNPs dispersed into the PLA network, more hydrophobic/hydrophobic interactions between PLA and oleic acids and even less ordered methyl groups (PLA) on the film surface. Hence, the measured surface water CA decreased to ∼70.8°, indicating the further improved water wettability and leading to the enhanced hydrolysis of PLA (Figure 3c, c-1 and c-2; Figure 4c, c-1 and c-2). Nevertheless, the dramatic difference in the peak intensities observed in the in situ SFG spectra of pure PLA and PLA−NPs2 films (Figure 5b) also implies that the incremental dispersion of MNPs in the PLA system highly increased the disordering of the whole system and thus lowered the crystallinity of PLA on the surface during the water contact (Figure 6c). This in turn facilitated the water−sample interactions and led to enhanced hydrolysis of PLA as the MNPs concentration increased to ∼20%.

However, in the case of PLA−NPs3, the trend of PLA hydrolysis variation was opposite to that of PLA−NPs1 and PLA−NPs2 films: Slower hydrolysis was observed by SEM (Figure 3d, d-1, d-2 and d-3) and AFM (Figure 4d, d-1 and d-2). Surface CA and in situ SFG results can also be well correlated to the SEM observation. For CA, the surface CA increased to 73.4° rather than further decrease compared to that of PLA−NPs2. Because of the high MNP concentration (∼50%), the aggregation of MNPs may happen (Figure 6d). The MNP aggregation led to the formation of MNP clusters, in addition to the well dispersed MNPs. The concentration of dispersed MNPs may be higher than ∼2% but lower than ∼20%. Likely the dispersed MNPs present in the surface region

DOI: 10.1021/acsami.5b02210
ACS Appl. Mater. Interfaces 2015, 7, 9410−9419

Table 2. PTX Release Rates at Different Times and the Ratios between Those of PLA−MNP Composites and Those of Pure PLA Films

samples / PTX release	0.5 h (%)	times	1 h (%)	times	39 h (%)	times	60 h (%)	times
PLA	0.06	N/A	6.07	N/A	19.93	N/A	30.73	N/A
PLA−NPs1	5.48	91.33	8.63	1.42	23.72	1.19	33.82	1.10
PLA−NPs2	13.21	220.17	21.93	3.61	53.96	2.71	59.22	1.93
PLA−NPs3	5.32	88.67	7.80	1.29	32.66	1.64	40.89	1.33

affect surface wettability. This interpretation could be supported by CA results. For SFG data, different from the cases of PLA−NPs1 and PLA−NPs2 where the hydrophobic and hydrophobic interactions between PLA and oleic acid (NPs) resulted in less methyl groups ordered on the surface, here for PLA−NPs3, MNP clusters on or near the surface may have induced more ordered PLA domains and thus higher peak intensities were observed in the SFG spectrum of PLA−NPs3 before hydrolysis (Figure 5a). After contacting with water, the PLA domains between MNPs clusters may have higher crystallinity compared to other three films, so the hydrolysis was hindered.

Two possible factors may determine the hydrolysis behavior on the PLA sample surfaces. One is the hydrophobic/hydrophobic interaction between PLA and oleic acid molecules on MNPs, which changes the surface CA and water wettibility, and thus affects the interaction between water and polymer films. The other is the formation of crystalline-like PLA domains on the surface in the presence of water molecules. Such a highly ordered structure was found to be more resistant to water and thus inhibited PLA hydrolysis.[36,37] These two mechanisms were found to work synergistically to mediate the hydrolysis processes of PLA as the MNP concentration was varied.

3.4. PTX Controlled Release. To further understand the hydrolysis behaviors of PLA and PLA−NP hybrid films, a hydrophobic antitumor drug PTX was loaded into four kinds of PLA samples to examine the corresponding drug release rate. Figure 7 shows the cumulative release rate of loaded PTX released from four PLA and PLA−MNP hybrid samples. The time-dependent drug release rates for all the samples have similar features: The initial release rate of PTX was high during the first few hours, followed by a slower release in the next few days. Note that the time-dependent release rates in the first 3 h were enlarged in the inset of Figure 7. The results demonstrate that PTX PLA films with different MNP concentrations show different PTX release rate features. On the whole, the PTX PLA films with MNPs have higher PTX release rate than pure PLA film; especially when MNP concentration was 20%, the PTX release rate can be enhanced significantly. In order to further understand the release mechanism, Table 2 lists the release rates for these four types of samples after 0.5, 1, 39, and 60 h hydrolysis. The release rate of PTX from pure PLA was low; after 0.5 h, only 0.06% drug was released. Even after 60 h, only 30.73% PTX was released. This is consistent with our discussion above that the intrinsic hydrolysis rate of PLA is slow. After adding ∼2% MNPs into PLA, the drug release rate was largely increased to ∼90 times greater in the first 0.5 h, which is reasonable because the better surface wettibility induced by MNPs allowed more rapid diffusion of the aqueous release medium into the film, which led to more effective dissolution and extraction from the surface and subsurface of the polymer than pure PLA at the beginning. However, after hydrolysis happened, the formation of crystalline-like structures on/near the surface caused the hydrolysis process to become slow. Hence after 1 h, the drug release rate was quite similar to that of pure PLA, only increased by ∼50%. As the release time increased to 39 and 60 h, the rate differences between the pure PLA and PLA−NPs1 samples became smaller. The release rates from PLA−NPs1 were only 19% and 10% greater than that of pure PLA. In the case of PLA−NPs2, the trend of the time-dependent drug release rate increase is very similar to the PLA−NPs1 case. As expected, the PTX release rate was greatest for PLA−NPs2 (the ∼20% MNP sample). After 0.5 h, 13.21% PTX was released from PLA−NPs2, which is ∼220 times greater than that of pure PLA. While, after1 h, the release rate of PTX was 21.93%, which is reduced to 3.61 times of pure PLA. After 60 h, about 60% of the PTX was released from the PLA−NPs2 sample, and the release rate of PTX was 2 times that of PLA. For PLA−NPs3 sample, until after 1 h, there is only 7.80% PTX released from the composite film. These drug release results are very consistent with SEM, AFM, CA, and SFG data, and can be explained by the two possible factors which we discussed above.

When 50% MNPs were mixed with PLA, in the first 30 min, the release rate of PTX from the PLA−NPs3 sample was at a similar level as that of the PLA−NPs1 sample, but much lower than that of PLA−NPs2 and ∼88 times greater than that of pure PLA. Nevertheless, the release rate was 32.66% after 39 h, which is higher than that of PLA and PLA−NPs1, but still lower than that of PLA−NPs2. The early stage of PTX release from PLA−NPs3 can be explained by our previous discussion. However, as time increased, some MNP clusters were removed from the sample, thus the new surface would have some new pores formed by MNPs which would improve the liquid-uptake and the drug release. The overall drug release process of PLA−NPs3 is faster than that of PLA−NPs1 after 60 h. The PTX release results indicate that excellent drug controlled release function can be achieved when MNP concentration is about 20% in the PLA−MNP composite film. That is, at the beginning, when the delivery system reaches the targeted tissue, the drug can be released as quickly as possible to reach the effective level for therapy. Then, for a prolonged period of time, the drug concentration can be maintained at an effective level, and the drug can be released in a controllable way. This is the ideal drug release mode for most drug delivery scenarios.

4. CONCLUSIONS

In summary, we demonstrated that through engineering PLA with various amounts of MNPs, it is feasible to control the embedded drug release rate. There were not only differences in physical surface appearance among the various PLA−MNP samples for different MNP concentrations, but also differences in drug release behavior. The different drug release behaviors are caused by the different PLA hydrolysis rates, which are induced by the differed surface wettability and surface

DOI: 10.1021/acsami.5b02210
ACS Appl. Mater. Interfaces 2015, 7, 9410−9419

crystallization due to different interactions between PLA and MNPs in various samples. When the MNP concentration in the PLA film is around 20%, the drug release rate could be increased up to 220 times in the first half hour during water exposure, which is beneficial for improving the controlled drug release characteristics in real application. When the PLA−NP composite contained above 50% MNPs, some MNPs aggregated in the sample, resulting in more surface crystalline and lower hydrolysis. More importantly, since the MNPs used in this study were proven to be effective ultrasound and magnetic resonance dual contrast agents, the PLA−MNP composite drug-delivery system engineered here should have promising multiple-functional applications in the future. Also, the methodology developed in this research to study the hydrolysis of the PLA and MNP system at the molecular level is general and can be extended to investigate other polymer and NP systems for drug delivery and beyond.

■ ASSOCIATED CONTENT

Supporting Information

Mean pore density and size results of PLA and PLA−MNPs hybrid films after hydrolysis. Surface topography of the AFM and cross-section surface profile before and after 1 h hydrolysis. Static water contact angle of PLA−MNPs hybrid films before and after water hydrolysis. SFG ssp spectra collected from the surfaces of (a) pure PLA film, and PLA−MNP composites with different MNP bulk concentrations before and after water immersion for hydrolysis. This material is available free of charge via the Internet at http://pubs.acs.org.

■ AUTHOR INFORMATION

Corresponding Authors

*E-mail: xiaoxian@umich.edu (X.Z.).
*E-mail: zhanc@umich.edu (Z.C.).
*Phone: +86 25 83272460. Fax: +86 25 83272460.+49 89 289 12 473. E-mail: guning@seu.edu.cn. (N.G.).

Author Contributions

§The manuscript was written through the contributions of all authors. All authors have given approval to the final version of the manuscript. The authors declare no competing financial interest. These authors contributed equally.

Notes

The authors declare no competing financial interest.

■ ACKNOWLEDGMENTS

The authors would like to thank Mr. Joshua A. Jasensky for useful discussion. The authors acknowledge the support from the project of National Key Basic Research Program of China (Nos. 2011CB933503 and 2013CB733804), National Natural Science Foundation of China (Nos. 31370019 and 61127002), Natural Science Foundation of Jiangsu Province (No. BK2011036), Foundation for the Author of National Excellent Doctoral Dissertation of PR China (No. 201259), the Fundamental Research Funds for the Central Universities, as well as the University of Michigan.

■ ABBREVIATIONS

PLA, poly(lactic acid)
NP, nanoparticle
MNP, magnetic nanoparticles
SEM, scanning electron microscopy
CA, contact angle goniometry
SFG, sum frequency generation
SPIO, superparamagnetic iron oxide Fe_3O_4 NPs
QDs, CdTe quantum dots
PTX, paclitaxel

■ REFERENCES

(1) Lee, W. K.; Gardella, J. A. Hydrolytic Kinetics of Biodegradable Polyester Monolayers. *Langmuir* **2000**, *16*, 3401−3406.
(2) Chandorkar, Y.; Bhagat, R. K.; Madras, G.; Basu, B. Crosslinked, Biodegradable, Cytocompatible Salicylic Acid Based Polyesters for Localized, Sustained Delivery of Salicylic Acid—An in Vitro Study. *Biomacromolecules* **2014**, *15*, 863−875.
(3) Way, C.; Wu, D. Y.; Cram, D.; Dean, K.; Palombo, E. Processing Stability and Biodegradation of Polylactic Acid (PLA) Composites Reinforced with Cotton Linters or Maple Hardwood Fibres. *J. Polym. Environ.* **2013**, *21*, 54−70.
(4) Anderson, J. M.; Shive, M. S. Biodegradation and Biocompatibility of PLA and PLGA Microspheres. *Adv. Drug Delivery Rev.* **2012**, *64*, 72−82.
(5) Luk, B. T.; Zhang, L. Current Advances in Polymer-Based Nanotheranostics for Cancer Treatment and Diagnosis. *ACS Appl. Mater. Interfaces* **2014**, *6*, 21859−21873.
(6) Lee, W. L.; Loo, S. C. J. Revolutionizing Drug Delivery Through Biodegradable Multilayered Particles. *J. Drug Targeting* **2012**, *20*, 633−647.
(7) Ling, Y.; Wei, K.; Luo, Y.; Gao, X.; Zhong, S. Dual Docetaxel/Superparamagnetic Iron Oxide Loaded Nanoparticles for Both Targeting Magnetic Resonance Imaging and Cancer Therapy. *Biomaterials* **2011**, *32*, 7139−7150.
(8) Tian, B.; Shankarappa, S. A.; Chang, H. H.; Tong, R.; Kohane, D. S. Biodegradable Mesostructured Polymer Membranes. *Nano Lett.* **2013**, *13*, 4410−4415.
(9) Shenhar, R.; Norsten, T. B.; Rotello, V. M. Polymer-Mediated Nanoparticle Assembly: Structural Control and Applications. *Adv. Mater.* **2005**, *17*, 657−669.
(10) Ye, F.; Barrefelt, Å.; Asem, H.; Abedi-Valugerdi, M.; El-Serafi, I.; Saghafian, M.; Abu-Salah, K.; Alrokayan, S.; Muhammed, M.; Hassan, M. Biodegradable Polymeric Vesicles Containing Magnetic Nanoparticles, Quantum Dots and Anticancer Drugs for Drug Delivery and Imaging. *Biomaterials* **2014**, *35*, 3885−3894.
(11) Yao, Y.; Metwalli, E.; Moulin, J. F.; Su, B.; Opel, M.; Müller-Buschbaum, P. Self-Assembly of Diblock Copolymer−Maghemite Nanoparticle Hybrid Thin Films. *ACS Appl. Mater. Interfaces* **2014**, *6*, 18152−18162.
(12) Nicolas, J.; Mura, S.; Brambilla, D.; Mackiewicz, N.; Couvreur, P. Design, Functionalization Strategies and Biomedical Applications of Targeted Biodegradable/Biocompatible Polymer-Based Nanocarriers for Drug Delivery. *Chem. Soc. Rev.* **2013**, *42*, 1147−1235.
(13) Cao, Z.; Yu, Q.; Xue, H.; Cheng, G.; Jiang, S. Nanoparticles for Drug Delivery Prepared From Amphiphilic PLGA Zwitterionic Block Copolymers with Sharp Contrast in Polarity Between Two Blocks. *Angew. Chem., Int. Ed.* **2010**, *122*, 3859−3864.
(14) He, W.; Yang, F.; Wu, Y.; Wen, S.; Chen, P.; Zhang, Y.; Gu, N. Microbubbles with Surface Coated by Superparamagnetic Iron Oxide Nanoparticles. *Mater. Lett.* **2012**, *68*, 64−67.
(15) Yang, F.; Li, Y.; Chen, Z.; Zhang, Y.; Wu, J.; Gu, N. Superparamagnetic Iron Oxide Nanoparticle-Embedded Encapsulated Microbubbles as Dual Contrast Agents of Magnetic Resonance and Ultrasound Imaging. *Biomaterials* **2009**, *30*, 3882−3890.
(16) Gupta, A. K.; Gupta, M. Synthesis and Surface Engineering of Iron Oxide Nanoparticles for Biomedical Applications. *Biomaterials* **2005**, *26*, 3995−4021.
(17) Nunes, J.; Herlihy, K. P.; Mair, L.; Superfine, R.; DeSimone, J. M. Multifunctional Shape and Size Specific Magneto−Polymer Composite Particles. *Nano Lett.* **2010**, *10*, 1113−1119.
(18) Bertrand, N.; Leroux, J. C. The Journey of a Drug-Carrier in the Body: an Anatomo-Physiological Perspective. *J. Controlled Release* **2012**, *161*, 152−163.

DOI: 10.1021/acsami.5b02210
ACS Appl. Mater. Interfaces 2015, 7, 9410−9419

(19) Ford Versypt, A. N.; Pack, D. W.; Braatz, R. D. Mathematical Modeling of Drug Delivery from Autocatalytically Degradable PLGA Microspheres—A Review. *J. Controlled Release* **2013**, *165*, 29−37.
(20) Nishida, H.; Yamashita, M.; Nagashima, M.; Hattori, N.; Endo, T.; Tokiwa, Y. Theoretical Prediction of Molecular Weight on Autocatalytic Random Hydrolysis of Aliphatic Polyesters. *Macromolecules* **2000**, *33*, 6595−6601.
(21) Alves, N. M.; Pashkuleva, I.; Reis, R. L.; Mano, J. F. Controlling Cell Behavior Through the Design of Polymer Surfaces. *Small* **2010**, *6*, 2208−2220.
(22) Nguyen, P. N.; Nikolova, G.; Polavarapu, P.; Waton, G.; Phuoc, L. T.; Pourroy, G.; Krafft, M. P. Compressible Multi-Scale Magnetic Constructs: Decorating the Outer Surface of Self-Assembled Microbubbles with Iron Oxide Nanoparticles. *RSC Adv.* **2013**, *3*, 7743−7746.
(23) Fredenberg, S.; Jönsson, M.; Laakso, T.; Wahlgren, M.; Reslow, M.; Axelsson, A. Development of Mass Transport Resistance in Poly (Lactide-*co*-Glycolide) Films and Particles—A Mechanistic Study. *Int. J. Pharm.* **2011**, *409*, 194−202.
(24) Burkersroda, F. v.; Schedl, L.; Göpferich, A. Why Degradable Polymers Undergo Surface Erosion or Bulk Erosion. *Biomaterials* **2002**, *23*, 4221−4231.
(25) Álvarez, Z.; Mateos-Timoneda, M. A.; Hyroššová, P.; Castaño, O.; Planell, J. A.; Perales, J. C.; Engel, E.; Alcántara, S. The Effect of the Composition of PLA Films and Lactate Release on Glial and Neuronal Maturation and the Maintenance of the Neuronal Progenitor Niche. *Biomaterials* **2013**, *34*, 2221−2233.
(26) Codari, F.; Lazzari, S.; Soos, M.; Storti, G.; Morbidelli, M.; Moscatelli, D. Kinetics of the Hydrolytic Degradation of Poly (Lactic Acid). *Polym. Degrad. Stab.* **2012**, *97*, 2460−2466.
(27) Chen, Z. Understanding Surfaces and Buried Interfaces of Polymer Materials at the Molecular Level Using Sum Frequency Generation Vibrational Spectroscopy. *Polym. Int.* **2007**, *56*, 577−587.
(28) Chen, Z. Investigating Buried Polymer Interfaces Using Sum Frequency Generation Vibrational Spectroscopy. *Prog. Polym. Sci.* **2010**, *35*, 1376−1402.
(29) Chen, Z.; Shen, Y.; Somorjai, G. A. Studies of Polymer Surfaces by Sum Frequency Generation Vibrational Spectroscopy. *Annu. Rev. Phys. Chem.* **2002**, *53*, 437−465.
(30) Chen, S.; Li, L.; Zhao, C.; Zheng, J. Surface Hydration: Principles and Applications Toward low-Fouling/Nonfouling Biomaterials. *Polymer* **2010**, *51*, 5283−5293.
(31) Ye, H.; Abu-Akeel, A.; Huang, J.; Katz, H. E.; Gracias, D. H. Probing Organic Field Effect Transistors in situ During Operation Using SFG. *J. Am. Chem. Soc.* **2006**, *128*, 6528−6529.
(32) Wang, J.; Woodcock, S. E.; Buck, S. M.; Chen, C.; Chen, Z. Different Surface-Restructuring Behaviors of Poly (methacrylate)s Detected by SFG in Water. *J. Am. Chem. Soc.* **2001**, *123*, 9470−9471.
(33) Zhang, X.; Zhang, C.; Hankett, J. M.; Chen, Z. Molecular Surface Structural Changes of Plasticized PVC Materials after Plasma Treatment. *Langmuir* **2013**, *29*, 4008−4018.
(34) Anastasiadis, S. H. Development of Functional Polymer Surfaces with Controlled Wettability. *Langmuir* **2013**, *29*, 9277−9290.
(35) Zhang, X.; Chen, Z. Observing Phthalate Leaching from Plasticized Polymer Films at the Molecular Level. *Langmuir* **2014**, *30*, 4933−4944.
(36) Kawai, T.; Neivandt, D. J.; Davies, P. B. Sum Frequency Generation on Surfactant-Coated Gold Nanoparticles. *J. Am. Chem. Soc.* **2000**, *122*, 12031−12032.
(37) Lu, X.; Clarke, M. L.; Li, D.; Wang, X.; Xue, G.; Chen, Z. A Sum Frequency Generation Vibrational Study of the Interference Effect in Poly (*n*-butyl methacrylate) Thin Films Sandwiched Between Silica and Water. *J.Phys. Chem.C* **2011**, *115*, 13759−13767.
(38) Ding, A. G.; Shenderova, A.; Schwendeman, S. P. Prediction of Microclimate pH in Poly (lactic-*co*-glycolic acid) Films. *J. Am. Chem. Soc.* **2006**, *128*, 5384−5390.
(39) Johnson, C. M.; Sugiharto, A. B.; Roke, S. Surface and Bulk Structure of Poly-(lactic acid) Films Studied by Vibrational Sum Frequency Generation Spectroscopy. *Chem. Phys. Lett.* **2007**, *449*, 191−195.
(40) Iwata, T.; Doi, Y. Morphology and Enzymatic Degradation of Poly (L-lactic acid) Single Crystals. *Macromolecules* **1998**, *31*, 2461−2467.
(41) Bao, R. Y.; Yang, W.; Jiang, W. R.; Liu, Z. Y.; Xie, B. H.; Yang, M. B. Polymorphism of Racemic Poly (L-lactide)/ Poly (D-lactide) Blend: Effect of Melt and Cold Crystallization. *J.Phys. Chem.B* **2013**, *117*, 3667−3674.

DOI: 10.1021/acsami.5b02210
ACS Appl. Mater. Interfaces 2015, 7, 9410−9419